2010 IEEE International Conference on Robotics and Automation
Anchorage Convention District
May 3-8, 2010, Anchorage, Alaska, USA

Development of a Pneumatic Robot for MRI-guided Transperineal Prostate Biopsy and Brachytherapy: New Approaches

Sang-Eun Song, Nathan B. Cho, Gregory Fischer, Nobuhito Hata, Clare Tempany, Gabor Fichtinger and Iulian Iordachita

Abstract—**Magnetic Resonance Imaging (MRI) guided prostate biopsy and brachytherapy has been introduced in order to enhance the cancer detection and treatment. For the accurate needle positioning, a number of robotic assistants have been developed. However, problems exist due to the strong magnetic field and limited workspace. Pneumatically actuated robots have shown the minimum distraction in the environment but the confined workspace limits optimal robot design and thus controllability is often poor. To overcome the problem, a simple external damping mechanism using timing belts was sought and a 1-DOF mechanism test result indicated sufficient positioning accuracy. Based on the damping mechanism and modular system design approach, a new workspace-optimized 4-DOF parallel robot was developed for the MRI-guided prostate biopsy and brachytherapy. A preliminary evaluation of the robot was conducted using previously developed pneumatic controller and satisfying results were obtained.**

I. Introduction

PROSTATE cancer is a major health concern in the United States. In 2009, an estimate of 192280 new cases and 27360 deaths are reported, which are the largest number of male cancer (25%) and the second largest cause of cancer death (9%) for men. In the last two decades, however, the death rate is decreasing, which largely reflects improvements in early detection and/or treatment [1]. A typical diagnosis method for prostate cancer is core needle biopsy. Once cancer is found, low-dose-rate (LDR) permanent brachytherapy is commonly performed by implanting a large number (50-150) of radioactive seeds into the prostate using needles [2]. The distribution of seeds is important since it should effectively cover suspected volume in order to eradicate cancer with minimal radiation toxicity to healthy tissues.

Transrectal ultrasound (TRUS) guidance is the most commonly used navigation method for the biopsy and brachytherapy since the simple method is utilizing real-time imaging at low cost [3]. TRUS-guided biopsy, however, has a poor cancer detection rate of 20%-30% [4]. In order for greater detection rate, magnetic resonance imaging (MRI) has been sought for the prostate procedures. MRI has high sensitivity for detecting prostate tumor (excellent soft tissue contrast), high spatial resolution, and multi-planar volumetric imaging capabilities [5]. However, closed-bore high-field (1.5T or greater) MRI has not been widely adopted for prostate interventions due to strong magnetic field that requires MRI-compatibility of surgical devices and physical limitation of in-bore access and workspace.

A clinical feasibility of MRI-guided prostate biopsy and brachytherapy was demonstrated by D'Amico *et al*. at the Brigham and Women's Hospital using a 0.5T open-MRI scanner to plan and monitor Transrectal needle placement [6], [7]. The needles were inserted manually using a plastic guide that has a grid of holes similar to the TRUS-guided procedure. Zangos *et al*. used a transgluteal approach with 0.2T MRI but did not target the tumor foci [8]. Susil *et al*. reported four cases of transperineal prostate biopsy in a closed-bore scanner, where the patient (MRI table) was moved out of the bore for needle insertion, then, placed back into the bore for confirmation scan [9]. Beyersdorff *et al*. performed transrectal biopsy in a 1.5T MRI scanner with a passive articulated needle guide [10].

Early robotically assisted (guided) instrument placement in MRI has been investigated in neurosurgery [11] and percutaneous interventions [12], [13]. Chinzei *et al*. developed a general purpose robotic assistant for open-MRI [14] that was subsequently adapted for transperineal intraprostatic needle placement [15]. Krieger *et al*. presented a 2-DOF manually manipulated mechanical device to guide transrectal prostate biopsy [16]. In recent years, a number of MR-compatible motor technologies have been introduced: Stoianovici *et al*. developed a fully MRI-compatible pneumatic stepper motor called PneuStep [17], Elhawary *et al*. presented an air motor for limb localization [18], and Suzuki *et al*. introduced a stepper motor that uses the scanner's magnetic field as a driving force is described [19].

More recent robot developments include pneumatic stepping motors on a light needle puncture robot [20], the Innomotion pneumatic robot for percutaneous interventions [21], haptic interfaces for functional MRI (fMRI) [22], a fully automated prostate brachytherapy seed placement system (MrBot) using PneuStep [23], and a simple 2-DOF (2-DOF are actively controlled to date) transperineal prostate needle placement robot [24], which is an early 'proof-of-concept' robot of the current robot development. Fig. 1 shows the 2-DOF robot that provides manual sliding needle insertion, and clinical mockup with a custom made leg support.

This work is supported by National Institute of Health Grants: 1R01CA111288, 5P01CA067165 and 5U41RR019703.

S. Song, N. Cho and I. Iordachita are with National Science Foundation Engineering Research Center for Computer-Integrated Surgical System and Technology, The Johns Hopkins University, Baltimore, MD, US.

G. Fischer is with Worcester Polytechnic Institute, Worcester, MA, US

N. Hata and C. Tempany are with Brigham and Women's Hospital, Harvard Medical School, Boston, MA, US

Gabor Fichtinger is with Queen's University, Kingston, Canada.

Corresponding author: S. Song (e-mail: ssong17@jhu.edu)

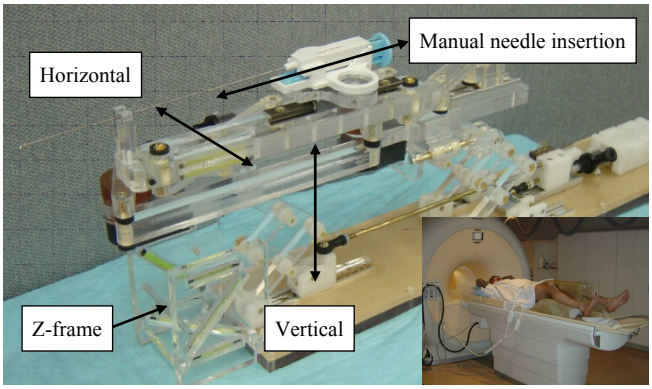

Fig. 1. 2-DOF needle guide robot, and clinical setup with custom made leg support (inset).

With a particular interest on highly MRI-compatible pneumatically actuated robotic systems developed for in-bore operation, this paper introduces a new robot development by understanding advantages and disadvantages of such robots, and investigating new strategic and engineering approaches towards optimized clinical implementation. MrBot [23] that uses a stepper motor type pneumatic actuator solving critical problems of controlling pneumatic actuation, and the 2-DOF robot prototype (Fig. 1), were often benchmarked for this new robot development. The following section (Section II) identifies robot requirements and new approaches in order to overcome known problems, and Section III details the materialization of the robot. Section IV describes preliminary evaluation of the robot and new approaches, followed by conclusion and future work (Section V).

II. System Identification: New Approaches

Key requirements that have been discussed from existing pneumatically actuated MRI-compatible robot developments can be summarized in a number of major challenges: design optimization, pneumatic actuator controllability enhancement, and adaptability in currently available clinical environment. A list of engineering and procedural approaches that could resolve such challenges were identified.

A. Operational Workspace

MrBot [23] is designed to position a patient in the decubitus position since the end-effector (needle tip) workspace is generated too high from the robot's base. Considering that usually diagnostic scans are obtained from the supine position, navigating deformable soft tissue targets in different pose intraoperatively could be a disadvantage. The 2-DOF robot [24], however, is designed to accommodate a patient in the supine position similar to conventional TRUS setup (workspace is described in [24]). In order to fit into the narrow 'between-legs' space, the robot was configured with scissor-like vertical manipulation mechanism. From the design, it was noticed that the unused 'under-legs' space can be utilized for robot space. Also, for the highly subjective workspace, a set of selectable links (in size and shape) can be used instead of a fixed link to optimize workspace and to minimize robot space within the limited space.

B. Kinematic Configuration and Structural Rigidity

Accessing entire volume of prostate via perineum may not be achievable with 2-DOF needle positioning since the insertion trajectory should avoid pubic arch and urethra. Anatomically, the avoidance can be achieved by adding 2-DOF (pitch and yaw angling). Hence, 4-DOF manipulation is required. In order to maximize the use of 'under-legs' space and minimize 'between-legs' space, a pyramid-shape robot structure was sought. To accommodate a long needle driving range and to satisfy the required manipulation, a 4-DOF parallel kinematic structure that has a coupled two planar manipulation was configured with ball joints shown as Fig. 2.

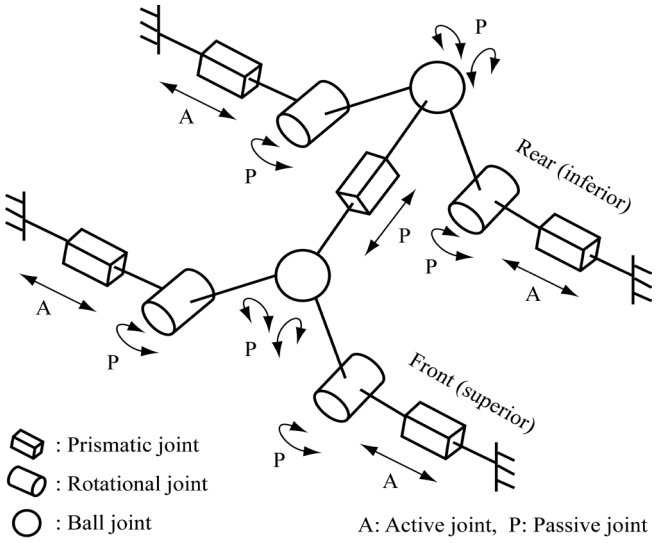

Fig. 2. Equivalent kinematic diagram of the robot.

The parallel structure is also beneficial for structural rigidity of the robot since it distributes reaction and/or external forces to more than one joint. Furthermore, a low friction air-cylinder driven joint that has no transmission reduction e.g. gear seems unsuitable for a serially linked robot, since it requires larger force (higher air pressure) to drive joints and to withstand overall robot structure in general.

C. Pneumatic Actuator Controllability

PneuStep [17] achieved high resolution position control of pneumatic actuation with its unique mechanism that delivers step-like manipulation. However, it is complex and costly. Another pneumatic actuator used for recent MRI-compatible robot developments is a custom made air cylinder that is modified from Airpel 9.3mm bore air cylinder (Airpel E9 Anti-Stiction Air Cylinder, Airpot Corp., Norwalk, CT, US). It has very low friction (as low as 0.01 N) and can apply forces up to 46.8 N. The pneumatic cylinder alone may be used for high precision control but to increase stability and controllability, a simple external damping mechanism that can stabilize cylinder's dynamic behavior, was sought. This type of system provides smooth movement, which is ideal for our case, and it eliminates many of the difficulties associated with servo control of a pneumatic cylinder. Previously, we have implemented a pneumatic actuator control algorithm as

a theoretical approach but it was not successful and not fully understandable due to the complexity and inconsistency. Instead, an experimental approach was chosen to overcome problems that exist in our previous development without major system alteration. The following section describes the test and results.

III. Robot Development

Based on the new approaches that are discussed in the previous section, a new MRI-compatible robot prototype was designed and fabricated. An experimental investigation on the external damping mechanism is first described. Then, details of the 4-DOF robot development are introduced. Also, other system components such as control hardware and planning software are briefly introduced.

A. Actuator Mechanism Evaluation

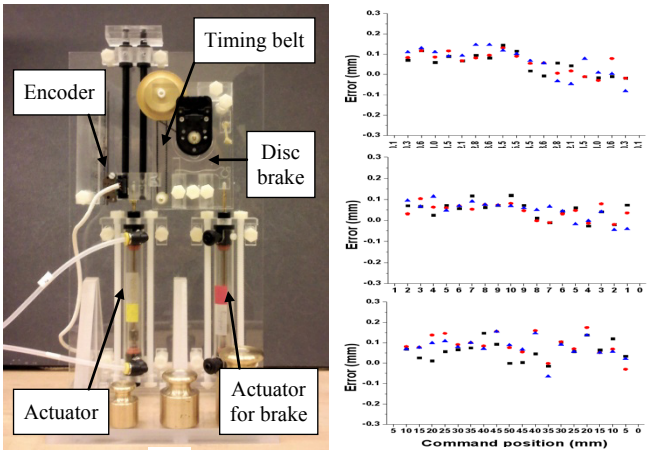

(a) (b)

Fig. 3. (a) 1-DOF test rig of the external damping mechanism (disc brake was not used for the tests), and (b) accuracy test results (top: 0.1-1.0 mm positioning, mid: 1mm positioning, bottom: 5mm positioning)

Timing belt and pulley mechanism was decided as an external damping since it can easily be MRI-compatible, damping can be roughly adjusted by changing the belt tension, and it has near-zero backlash, which is crucial because it disables the added damping effect at direction changes. Fig. 3 (a) shows the 1-DOF test rig. The test was to measure how accurate the actuator can achieve with the timing belt damping mechanism. A standard PID control was applied and gain values were tuned for the setting. A set of short (0.1 mm-1.0 mm), mid (every 1mm), and long (every 5mm) positioning tests were conducted. The target positions were evenly distributed upwards and downwards of the vertical setup in order to observe gravity influence.

Each test set was repeated three times and the resulting error values are shown in Fig. 3 (b). The Maximum error was 0.2 mm throughout all distance range with the average error value of 0.15 mm, which seems sufficient enough for the low cost pneumatic actuator with the simple timing belt. With the previous gain value, which was set without load, the same target positioning tests with various loads (weights of 100g, 200g, 300g and 400g) were also conducted. However, the actuator mostly failed to stop as it overshoots and continued to oscillate. In summary, the external damping mechanism seemed effective for the controllability enhancement of the pneumatic actuator. Appropriate gain value tuning is crucial and it seems very difficult to handle various loads with a fixed gain, which suggests that minimizing load variation could be a critical requirement for pneumatic robots.

B. 4-DOF Parallel Robot

As discussed in Section II-*B*, a 4-DOF parallel kinematic structure robot that is capable of guiding widely used biopsy and brachytherapy needles, was designed. Four pneumatic actuator units are located in the lower position to maximize the use of 'under-legs' space and two identical triangle shape parallel linkages are located at the front (superior) and rear (inferior) end of the robot for the narrow 'between-legs' space. Current robot design aimed to provide needle positioning only so that a simple rail-and-carriage sliding joint was temporarily designed to allow manual insertion. In future, however, this part will be replaced with a remote needle driver unit that provides haptic feedback, which is being done in parallel [25]. This also can utilize the robot for real-time MRI imaging e.g. advancing needle while scanning. Fig. 4 shows the robot CAD model (blue lines represent timing belts and arrows are axis direction).

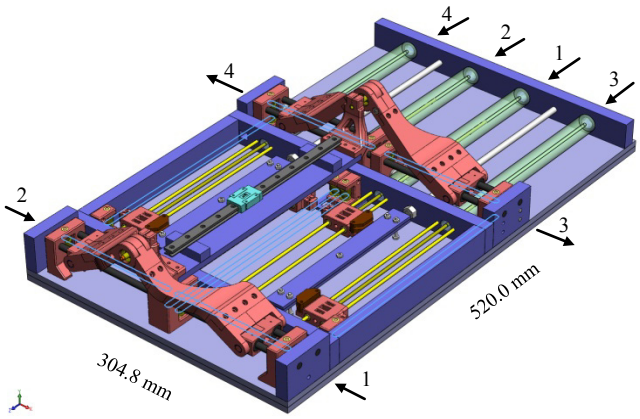

Fig. 4. CAD model of the 4-DOF robot with manual needle insertion slide.

Via timing belts and pulleys, each pneumatic cylinder actuation is transmitted to the prismatic manipulation of front and rear triangle structure, creating a planar manipulation respectively. The front ball joint is axially (needle platform axis) fixed and the rear ball joint is axially free sliding. The kinematic linkage of the two planar positioning subsequently delivers a 4-DOF needle guide. Fig. 5 illustrates the planar workspace of the identical front and rear triangle structure. A reachable kinematic workspace and a 50mm reference circle that fits into the coverage are shown. The workspace is determined by the actuator moving range, angle limit, and the link length L. The moving range and angle are limited by MRI table width but the link length is relatively easy to change as discussed in Section II-*A*. The maximum angle limit was set to avoid robot body collision and the minimum limit was set to prevent a large initial force, which was

problematic in the previous robot's scissor mechanism [24]. Each joint position J_n is determined using inverse kinematics. In Fig. 5, the joint position can be written as (1), where (x, y) is a target position on the plane, L is link length, and a is vertical offset.

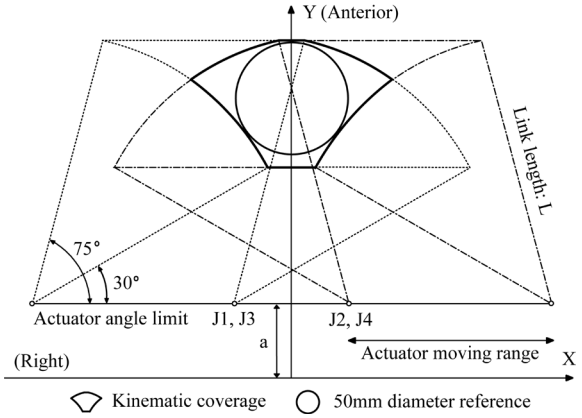

Fig. 5. Right-anterior sectional planar workspace of the robot when the front and rear triangle positioning is identical. L is 120 mm and the joint axis is 30 mm above the robot's base frame.

$$J_{1,3} = x + \sqrt{L^2 - (y-a)^2},\ J_{2,4} = x - \sqrt{L^2 - (y-a)^2} \qquad (1)$$

The robot fabrication materials are all non-ferrous. Most material is fully MRI-compatible plastic with a minimal amount of non-ferrous metal that was designed to avoid resonance (thus heating) and eddy currents to disturb field homogeneity. Also, the architecture, controller, and relevant parts are similar to the previous system that we have proven MRI-compatibility thoroughly [24]. In the CAD model, the blue colored parts are cast acrylic machined by laser cutter and the red colored parts were fabricated from commercial Stereolithography Apparatus (SLA) rapid-prototype service using Acura® 60 plastic (Acu-Cast Technologies, LLC., Lawrenceburg, TN). Plastic ball joints, bearings, and bushings are all off-the-shelf parts (Igus Inc., East Providence, RI). Non-ferromagnetic brass (alloy 260 and 360) and anodized aluminum (alloy 6061) shafts were also used.

Unlike other in-bore robots that are single-bodied and physically separated from patient, this robot was designed in a number of detachable modules: base, manipulator, and registration block. The base module provides a rigid flat base for the robot and also it could reduce the necessity of re-registration since the patient is located on the base. The registration block module was designed to locate the tracking fiducial frame (descried in [24]) close to the prostate. Also, the frame can be removed after registration since it becomes an obstacle in the limited workspace. If re-registration is required, only the module needs to be repositioned to a designated position on the base module. Fig. 6 shows the fabricated robot.

C. Controller and Navigation Software

The controller described in [24] is also used for the new robot. It previously operated inside of the scanner room, approximately 3 m from the 3-T scanner without functional difficulties or significant image quality degradation. The controller that is in the EMI shielded enclosure contains the embedded Linux PC providing low-level servo control, the piezoelectric valves, and the fiber-optic Ethernet converter. Connections to the robot include the air hose, the encoder cable. The controller is powered through the grounded patch panel, which is designed for such connections and data communication is enabled via fiber-optic Ethernet.

3-D Slicer (www.slicer.org) surgical navigation software serves as a user interface with the robot. The navigation software is running on a Linux-based workstation in the scanner's console room, which is connected to the robot via Ethernet. A customized graphical user interface (GUI) specially designed for the prostate intervention is used with the robot, which is described in [26].

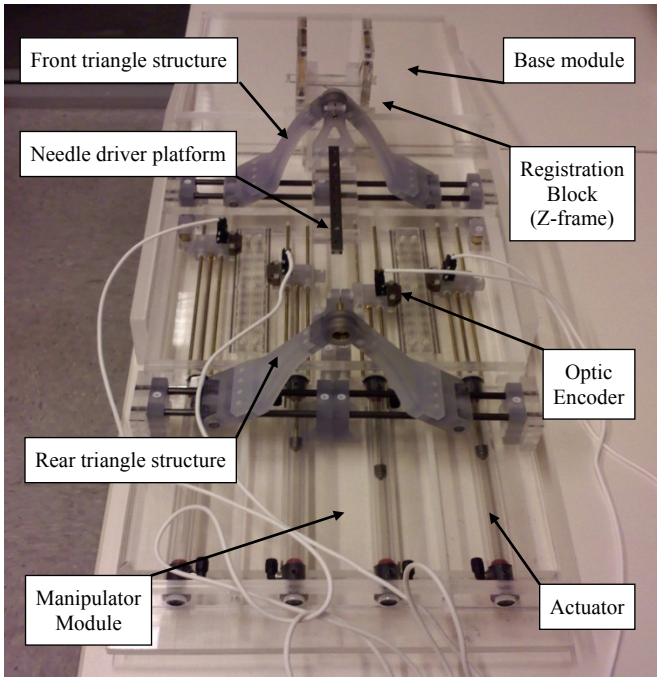

Fig. 6. Robot manufactured with acrylic and plastic rapid prototype.

IV. Mechanism and Design Evaluation

Preliminary engineering evaluation of the new robot was conducted to quantify the outcome of the external damping added actuator mechanism and the parallel robot structure. Since the on-going robot development is in new design evaluation stage, joint space controllability was focused, where physical movements are directly digitized by high resolution (2000 counts per inch i.e. 0.0127 mm linear resolution) optic encoders. Also, in order to confirm the feasibility and integration of the modular robot with the current navigation software and MRI scanner room environment, an engineering mockup using a prostate phantom was carried out.

A. Control Accuracy

For the robot control accuracy test, each actuator was tuned. First, in order to eliminate backlash, timing belts were tensioned by extending the distance between pulleys. Then, control parameters i.e. proportional, integral, and derivative

gains were individually set for the highest possible positioning accuracy. Thereafter, a set of 9 target positions that are evenly spread around within the robot's Right-anterior planar workspace, i.e. the axial image plane in MRI scan, were chosen. 8 targets are formed in a circle at every 45 degree and a target at the center of the circle. Although the robot can target larger volume by pitch and yaw angling, no such positioning was included in the test, since needle insertion depth information is required. Each actuator's required joint-space displacement was obtained using inverse kinematics. Then, the set was repeated six times at every 10 minutes in order to evaluate repeatability over the time period that the robot is operational in clinical procedure.

Each actuator's position error values over the entire experiments are shown in Fig. 7. The maximum error was found at 0.5 mm on the rear right actuator, which is greater than that of the 1-DOF test. The average joint-space (actuator) error was 0.2 mm, which is satisfying for this over-millimeter target accuracy application, and no significant variation was observed from all four actuators.

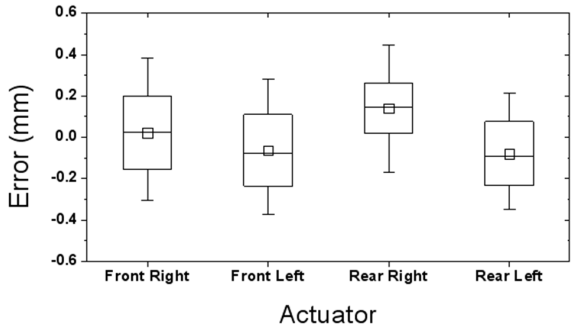

Fig. 7. Joint-space accuracy test result. 'Front' refers superior direction.

The actuator's position error contains complex kinematic interaction of the robot. Unlike the 1-DOF test, the robot actuator's accuracy can be affected by the kinematic situation. With a significant load (both external load and robot's structural load), this could be a crucial controllability problem, which is discussed as 'variable load on a fixed gain' in Section III-*A*. In order to observe the kinematic variation, the planar positioning results are plotted on the target circle as shown in Fig. 8. The mean error variation among the nine points was less than 0.11 mm. It seems that the parallel structure acts as damping to each actuator resulting in consistent positioning accuracy.

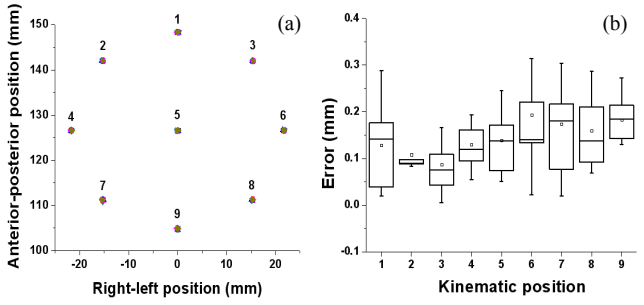

Fig. 8. Kinematic consistency plot: (a) shows the positioning results on 9 predefined targets, and (b) shows their error value variation.

The position errors in the front and rear triangular plane are accumulated towards the needle tip as it is projection of both errors. To estimate the needle tip error, which is the global positioning error of this robot, a projected needle tip error was ranged from the front and rear planar position error. Assuming that the deepest (superior) target in the prostate is within 150 mm distance from the front ball joint, a global positioning error stays within approximately 0.5 mm range. Fig. 9 illustrates the global needle tip position error range.

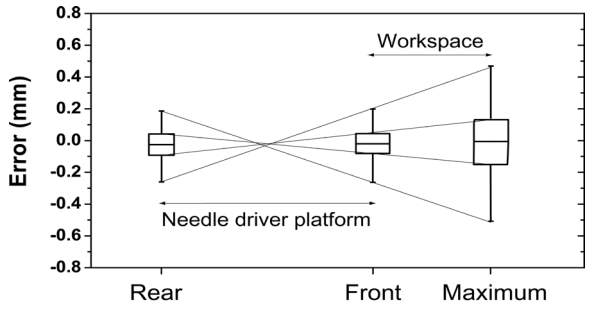

Fig. 9. Global needle positioning error range. Front and Rear represent ball joints that are 330 mm apart and Maximum is the needle insertion range.

B. Repeatability

Repeatability seems a less important property for surgical robots since they are not usually operated repeatedly over a long period of time and often recalibrated. However, it can be a substantial problem for the non-metallic pneumatic actuator because its mechanical behavior could easily be changed by temperature and humidity in a short period of time. Then, it introduces inconsistency in actuator's static and dynamic friction forces, which subsequently result in poor position accuracy. Nevertheless, it was not found over the entire experiment and as expected, it seemed that the external damping mechanism's mechanical property is far greater so that it governs the actuator's behavior eliminating the smaller inconsistency in the tests. Fig. 10 shows overall error values over the test period.

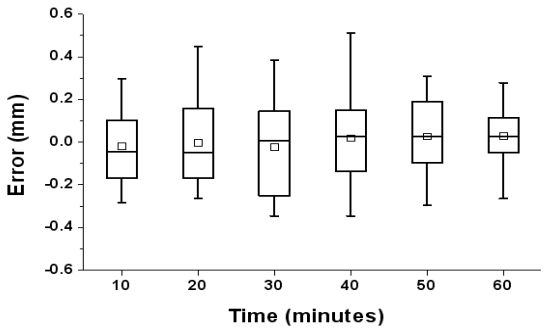

Fig. 10. Entire position error values per time. Tests were repeated over 60 minutes approximately, which is similar to the clinical procedure.

V. Conclusion and Future Work

In order to overcome problems of pneumatically actuated MRI-compatible prostate needle placement robots, a new controllability enhanced external damping mechanism was developed. A simple test rig was built to examine the mechanism and the results indicated sufficient pneumatic

control accuracy. Using the new mechanism and workspace optimization design approaches, a new 4-DOF needle guide robot was developed for prostate biopsy and brachytherapy needle placement. A preliminary evaluation of the robot was conducted with satisfying results. Also, an early mockup trial using a prostate phantom (see Fig. 11) was carried out with focuses on overall system integration i.e. communication between robot, planning software and scanner console, and procedural feasibility for clinical use. Consequently, the new mechanism and other design approaches seem well adopted. In order to further current development towards clinical implementation, a sterilization solution needs to be added, which includes replacement of the prototype level materials and parts. Also, an appropriate patient leg support that can also secure the designated workspace will be required. In a longer term, a needle driver module that provides haptic feedback will be developed to replace the manual needle insertion slide.

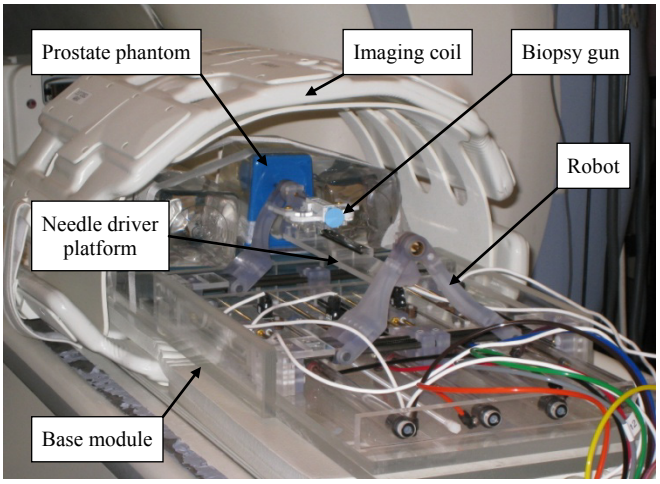

Fig. 11. A mockup setup for MRI guided robotic biopsy and brachytherapy.

REFERENCES

[1] A. Jemal, R. Siegel, E. Ward, Y. Hao, J. Xu, and M. Thun, "Cancer Statistics, 2009," in CA Cancer J Clin 2009; 59:225-249.

[2] J. C. Blasko, T. Mate, J. Sylvester, P. Grimm, and W. Cavanagh, "Brachytherapy for carcinoma of the prostate," Semin. Radiat. Oncol., vol. 12, no. 1, pp. 81–94, 2002.

[3] J. C. Presti, Jr., "Prostate cancer:Assessment of risk using digital rectal examination, tumor grade, prostate-specific antigen, and systematic biopsy," Radiol. Clin. North Amer., vol. 38, no. 1, pp. 49–58, 2000.

[4] M. K. Terris, E. M. Wallen, and T. A. Stamey, "Comparison of mid-lobe versus lateral systematic sextant biopsies in detection of prostate cancer,"Urol. Int., vol. 59, pp. 239–242, 1997.

[5] K. K. Yu and H. Hricak, "Imaging prostate cancer," in Radiol Clin North Am, vol. 38(1), pp. 59–85, 2000.

[6] A. V. D'Amico, R. Cormack, C. M. Tempany, S. Kumar, G. Topulos, H. M. Kooy, and C. N. Coleman, "Real-time magnetic resonance imageguided interstitial brachytherapy in the treatment of select patients with clinically localized prostate cancer," Int. J. Radiation Oncol., vol. 42, pp. 507–515, Oct. 1998.

[7] A. V. D'Amico, C.M. Tempany, R. Cormack, N. Hata, M. Jinzaki, K. Tuncali, M. Weinstein, and J. Richie, "Transperineal magnetic resonance image guided prostate biopsy," J. Urol., vol. 164, no. 2, pp. 385–387, 2000.

[8] S. Zangos, K. Eichler, K. Engelmann, M. Ahmed, S. Dettmer, C. Herzog, W. Pegios, A. Wetter, T. Lehnert, M. G. Mack, and T. J. Vogl, "MRguided transgluteal biopsies with an open low-field system in patients with clinically suspected prostate cancer: Technique and preliminary results," Eur. Radiol., vol. 15, no. 1, pp. 174–182, 2005.

[9] R. C. Susil, K. Camphausen, P. Choyke, E. R. McVeigh, G. S. Gustafson, H. Ning, R.W. Miller, E. Atalar, C. N. Coleman, and C.M´enard, "System for prostate brachytherapy and biopsy in a standard 1.5 T MRI scanner," Magn. Resonance Med., vol. 52, pp. 683–6873, 2004.

[10] D. Beyersdorff, A. Winkel, B. Hamm, S. Lenk, S. A. Loening, and M. Taupitz, "MR imaging-guided prostate biopsy with a closed MR unit at 1.5 T," Radiology, vol. 234, pp. 576–581, 2005.

[11] K. Masamune, E. Kobayashi, Y. Masutani, M. Suzuki, T. Dohi, H. Iseki, and K. Takakura, "Development of an MRI-compatible needle insertion manipulator for stereotactic neurosurgery," J. Image Guid. Surg., vol. 1, no. 4, pp. 242–248, 1995.

[12] A. Felden, J. Vagner, A. Hinz, H. Fischer, S. O. Pfleiderer, J. R. Reichenbach, and W. A. Kaiser, "ROBITOM-robot for biopsy and therapy of the mamma," Biomed. Tech. (Berl.), vol. 47 (Suppl. 1 Pt. 1), p. 2–5, 2002.

[13] E. Hempel, H. Fischer, L. Gumb, T. H¨ohn, H. Krause, U. Voges, H. Breitwieser, B. Gutmann, J. Durke, M. Bock, and A. Melzer, "An MRIcompatible surgical robot for precise radiological interventions," CAS, vol. 8, no. 4, pp. 180–191, Apr. 2003.

[14] K. Chinzei, N. Hata, F. A. Jolesz, and R. Kikinis, "MR compatible surgical assist robot: System integration and preliminary feasibility study," MICCAI, vol. 1935, pp. 921–933, Oct. 2000.

[15] S. P. DiMaio, S. Pieper, K. Chinzei, G. Fichtinger, C. Tempany, and R. Kikinis, "Robot assisted percutaneous intervention in open-MRI," in Proc. MRI Symp., 2004, p. 155.

[16] A. Krieger, R. C. Susil, C. Menard, J.A. Coleman,G. Fichtinger, E. Atalar, and L. L.Whitcomb, "Design of a novel MRI compatible manipulator for image guided prostate interventions," IEEE Trans. Biomed. Eng., vol. 52, no. 2, pp. 306–313, Feb. 2005.

[17] D. Stoianovici, A. Patriciu, D. Petrisor, D. Mazilu, and L. Kavoussi, "A new type of motor: Pneumatic step motor," IEEE/ASME Trans. Mechatron., vol. 12, no. 1, pp. 98–106, Feb. 2007.

[18] H. Elhawary, A. Zivanovic, M. Rea, Z. T. H. Tse, D. McRobbie, I. Young, B. D. M. Paley, and M. Lamprth, "A MR compatible mechatronic system to facilitate magic angle experiments in vivo," in Proc. Mid. Image Comput. Comput.-Assisted Interv. Conf. (MICCAI), Nov. 2007, pp. 604–611.

[19] T. Suzuki, H. Liao, E. Kobayashi, and I. Sakuma, "Ultrasonic motor driving method for EMI-free image in MR image-guided surgical robotic system," in Proc. IEEE Int. Conf. Intell. Robots Syst. (IROS), Oct. 2007, pp. 522–527.

[20] E. Taillant, J. Avila-Vilchis, C. Allegrini, I. Bricault, and P. Cinquin, "CT and MR compatible light puncture robot: Architectural design and first experiments," in Proc. Mid. Image Comput. Comput.-Assisted Interv. Conf. (MICCAI), 2004, vol. 3217, pp. 145–152.

[21] A. Melzer, B. Gutmann, T. Remmele, R. Wolf, A. Lukoscheck, M. Bock, H. Bardenheuer, and H. Fischer, "Innomotion for percutaneous image-guided interventions," vol. 27, pp. 66–73, May–June 2008.

[22] R. Gassert, R. Moser, E. Burdet, and H. Bleuler, "MRI/fMRI-compatible robotic system with force feedback for interaction with human motion," T. Mech., vol. 11, no. 2, pp. 216–224, Apr. 2006.

[23] D. Stoianovici, D. Song, D. Petrisor, D. Ursu, D. Mazilu, M. Mutener, M. Schar, andA. Patriciu, "'MRI Stealth' robot for prostate interventions," Minim. Invasive Ther. Allied Technol., vol. 16, no. 4, pp. 241–248, Jul. 2007.

[24] G. S. Fischer, I. Iordachita, C. Csoma, J. Tokuda, S. P. Dimaio, C. M. Tempany, N. Hata, and G. Fichtinger, "Mri-compatible pneumatic robot for transperineal prostate needle placement," Mechatronics, IEEE/ASME Transactions on, vol. 13, no. 3, pp. 295-305, 2008.

[25] H. Su, G. S. Fischer, A 3-Axis Optical Force/Torque Sensor for Prostate Needle Placement in Magnetic Resonance Imaging Environments, 2nd Annual IEEE International Conference on Technologies for Practical Robot Applications - TePRA 2009, Woburn, Massachusetts, November 2009.

[26] P. Mewes, J. Tokuda, S. P. DiMaio, G. S. Fischer, C. Csoma, D. G. Gobi, C. Tempany, G. Fichtinger, and N. Hata, "An integrated MRI and robot control software system for an MR-compatible robot in prostate intervention," in Proc. IEEE Int. Conf. Robot. Autom. (ICRA), May 2008.